2014

Effect of coastal-trapped waves and wind on currents and transport in the Gulf of California

Gutiérrez, Manuel O.

AGU PUBLICATIONS

JGR

Journal of Geophysical Research: Oceans

RESEARCH ARTICLE

10.1002/2013JC009538

Effect of coastal-trapped waves and wind on currents and transport in the Gulf of California

Manuel O. Gutiérrez[1], Manuel López[1], Julio Candela[1], Rubén Castro[2], Affonso Mascarenhas[3], and Curtis A. Collins[4]

[1]Departamento de Oceanografía Física, Centro de Investigación Científica y de Educación Superior de Ensenada (CICESE), Ensenada, Mexico, [2]Facultad de Ciencias Marinas, Universidad Autónoma de Baja California, Ensenada, Mexico, [3]Instituto de Investigaciones Oceanológicas, Universidad Autónoma de Baja California, Ensenada, Mexico, [4]Department of Oceanography, Naval Postgraduate School, Monterey, California, USA

Key Points:
- Upwelling CTWs increase the exchange in the Northern Gulf of California
- Wind fluctuations toward the mouth increase the exchange in the Northern Gulf

Correspondence to:
M. O. Gutiérrez,
gvillanu@cicese.edu.mx

Citation:
Gutiérrez, M. O., M. López, J. Candela, R. Castro, A. Mascarenhas, and C. A. Collins (2014), Effect of coastal-trapped waves and wind on currents and transport in the Gulf of California, *J. Geophys. Res. Oceans*, *119*, 5123–5139, doi:10.1002/2013JC009538.

Received 24 OCT 2013
Accepted 21 JUL 2014
Accepted article online 24 JUL 2014
Published online 12 AUG 2014

Abstract Subsurface pressure (SsP) observations from stations inside and outside of the Gulf of California (GC) are used to analyze the relationship between low-frequency currents, temperature, and transport inside the GC and intraseasonal coastal-trapped waves (CTWs), which propagate poleward along the coast toward the GC. Correlation functions and coherences of SsP stations were consistent with intraseasonal CTWs splitting in two at the mouth of the gulf: one part enters the gulf, propagates around the gulf, and eventually, toward the mouth, and another part that appears to "jump" the mouth of the gulf and travels poleward along the west coast of the peninsula. The correlation and coherence estimates of SsP at Manzanillo with currents showed that downwelling CTWs generated along-gulf current anomalies toward the head of the gulf at the mainland shelf of the mouth, whereas at Ballenas Channel sill (San Lorenzo sill) these waves generated current anomalies toward the mouth near the surface (bottom). At the San Lorenzo (SL) sill, downwelling CTWs increased the near-bottom (∼400 m) temperature and reduced the bottom transport of deep, fresher, and colder water that flows toward the head of the gulf. Cross-Calibrated Multiplatform winds were used to investigate their relationship with currents. The first empirical orthogonal function of the along-gulf wind stress showed that wind blowing toward the head of the gulf generated a reduction of bottom transport toward the head of the gulf through the SL sill, and intensified surface geostrophic current fluctuations toward the head of the gulf. There was also significant correlation between inflow bottom transport and outflow surface geostrophic velocities averaged across the gulf, consistent with the exchange pattern for the Northern Gulf.

1. Introduction

This study analyses the effects that the alongshore propagation of sea level anomalies and local winds within the Gulf of California (GC) have on currents, temperature, and transport in the GC. Several authors have shown poleward propagation of coastal-trapped waves (CTWs) along the eastern tropical Pacific coast and into the GC using tide gauges, moored observations, and numerical models [e.g., *Christensen et al.*, 1983; *Enfield and Allen*, 1983; *Enfield*, 1987; *Spillane et al.*, 1987; *Merrifield and Winant*, 1989; *Merrifield*, 1992; *Gjevik and Merrifield*, 1993; *Martínez and Allen*, 2004a, 2004b; *Zamudio et al.*, 2007, 2008, 2010]. For the range of periods of 4–20 days (synoptic band), these CTWs are generated by the alongshore wind stress generally associated with hurricanes and tropical storms that travel close to the Pacific coast of Mexico [*Enfield and Allen*, 1983; *Gjevik and Merrifield*, 1993; *Zamudio et al.*, 2010]. For periods of 30–90 days (intraseasonal band), the CTWs are generated in the western and central equatorial Pacific Ocean by atmospheric oscillations of similar periods [*Enfield*, 1987; *Spillane et al.*, 1987; *Zamudio et al.*, 2007, 2008]. Using a numerical model, *Martínez and Allen* [2004a, 2004b] showed that CTWs propagate into the GC along the mainland coast toward the sill zone where they split into two waves: one that propagates rapidly into the Northern Gulf and dissipates as a result of bottom friction, and a second wave, which reflects from the mid-riff islands and propagates along the peninsular side of the GC that carries most of the energy of the incident wave.

Intraseasonal CTWs have longer wavelengths, are more energetic, and are known to propagate into the GC, as well as poleward of the entrance of the GC along the western coast of the American continent up to the coast of California [*Enfield*, 1987; *Spillane et al.*, 1987]. The mechanism by which these waves propagate

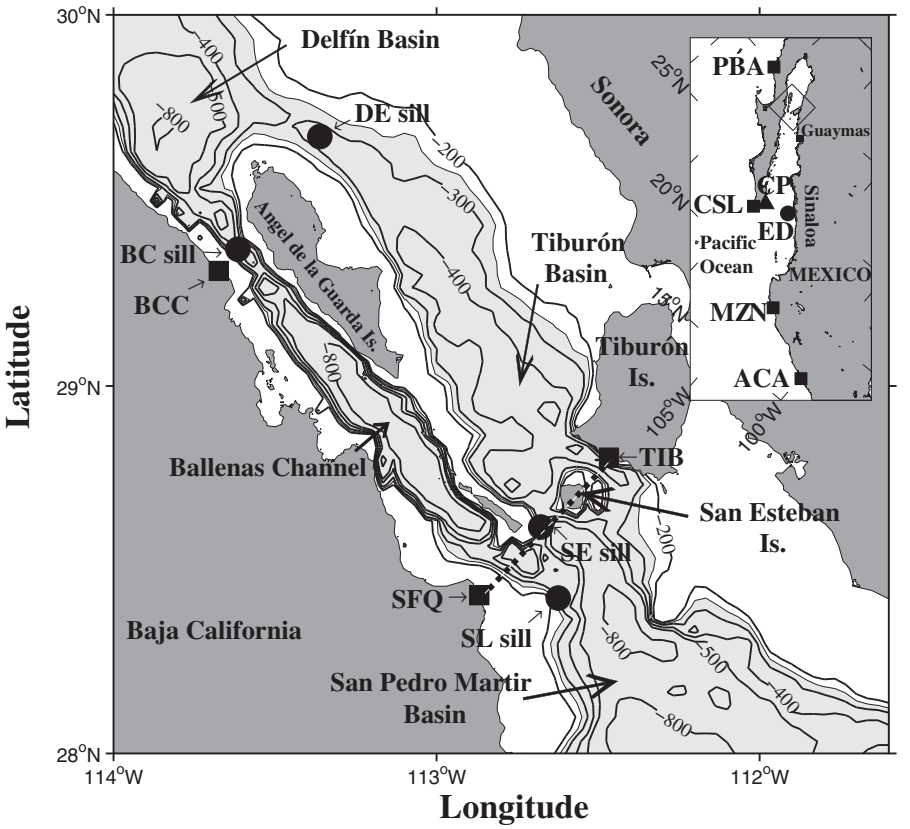

Figure 1. Map of the sill zone in the northern Gulf of California showing the bathymetry and the major basins of the area, with isobaths shown for depths of 200, 250, 300, 400, 500, 600 and 800 m (solid). The lightly shaded area shows depths greater than 250 m. Moored current observations (solid circle) and coastal subsurface pressure (solid square) stations are marked. Dotted line joins the two SsP stations (TIB and SFQ) where the surface geostrophic velocity was estimated. Inset at upper right is a map showing the locations of sea level stations along the Mexican Pacific coast, El Dorado (ED) mooring, and Cabo Pulmo (CP) meteorological station (solid triangle).

poleward across the mouth of the GC along the west side of the peninsula of Baja California is not known; however, it has been suggested that part of the wave can actually "jump" the mouth of the GC by some diffraction mechanism, rather than propagate around the GC [*Spillane et al*., 1987].

The propagation of CTWs within the gulf and their effect on currents and temperature has been less studied. This is particularly the case for the intraseasonal band, which requires longer time series. *Merrifield and Winant* [1989] analyzed currents and temperature in the Guaymas and Santa Rosalía shelves in the central GC and found no correlation with the local wind, but documented several energetic coastal-trapped wave (CTW) events, highlighting the importance of remote forcing. Possible evidence of CTWs that propagate around the gulf was only present in temperature and pressure observations on both sides of the gulf. However, given the different time lags of the correlations and the spatial structure of the temperature fluctuations, *Merrifield and Winant* [1989] and *Merrifield* [1992] attributed the temperature fluctuations to CTW-induced advection of cold waters from the sill region. These two studies focused mainly on the synoptic band, whereas some evidence of propagation around the gulf in the intraseasonal band was present in the phase lags found at both sides of the gulf [*Spillane et al*., 1987].

Similarly, there is little evidence of propagation or the possible effects of CTWs in the Northern Gulf, north of Tiburón Island (see Figure 1). *Zamudio et al*. [2010] did find some evidence that a CTW forced by hurricane Juliette reached the northernmost gulf. However, Juliette itself reached the northernmost gulf, so it was not clear what part of the response was due to a CTW forced outside of the GC, and what part was a locally forced response. Also, *López and García* [2003] found evidence of correlation between subsurface pressure and deep currents and temperature in the Northern Gulf with remote sea level at Manzanillo and Cabo San Lucas where some lags were consistent with propagation of CTWs.

The above studies show a strong remote forcing by CTWs within the GC. In this article, the effect of remotely forced CTWs on relatively long-term subsurface pressure (SsP), current, and temperature time series within the GC is investigated. Most of the observations within the GC were taken at the sills of the northern GC (NGC) so the effect of CTWs on the variability of the deep currents and transport entering the NGC could be determined. The near-bottom currents and transport at the sills constitute the strong lower layer inflow part of the exchange of the NGC [*López et al*., 2006, 2008, hereinafter *LCA* and *LCG*, respectively]. Furthermore, the relationship of local winds (within the GC) with currents and transport is briefly analyzed. In section 2, the observations are described. In section 3, data analysis is shown, and, in the section 4, the results are discussed and summarized.

2. Data

Hourly sea level data for 2002–2006 from coastal tide-gauges for Acapulco (ACA), Manzanillo (MZN), and Cabo San Lucas (CSL) were obtained from the University of Hawaii Sea Level Center (http://uhslc.soest.hawaii.edu/). Also, atmospheric pressure data referenced to mean sea level were obtained from the NCEP-NARR (National Centers for Environmental Prediction-North American Regional Reanalysis; http://www.esrl.noaa.gov/psd/data/gridded/data.narr.monolevel.html) product, which has spatial resolution of 30 by 30 km and a temporal resolution of 3 h. Bilinear interpolation was used to interpolate the gridded atmospheric pressure to the location of the tide gauges using four neighboring grid points, and 3 hourly data were then linearly interpolated to hourly intervals. Subsurface pressure (SsP) was then estimated using the sea level data and the atmospheric pressure with $P_a = \rho g \eta + P_{atm}$, where P_a is subsurface pressure in Pa, ρ is seawater density (1025 kg m^{-3}), g is gravity, η is the sea level in meters, and P_{atm} is the atmospheric pressure in Pa with its temporal mean removed. For convenience, P_a was converted to hPa.

Following *Spillane et al*. [1987], data gaps of up to 13 days in the SsP series were interpolated in two different ways. Short data gaps of up to 12 h were linearly interpolated. For longer data gaps of up to 13 days, a linear regression model using two neighboring stations was used. Residues of the SsP series were obtained after eliminating annual, semiannual, and tidal frequencies using harmonic analysis with the t_tide package [*Pawlowicz et al*., 2002]. However, since residues still contain some tidal and high-frequency variability, lagged-maximum correlations for the regression model were computed with a low-passed filtered version of the residues using the PL64 filter [*Limeburner*, 1985]. The lags of maximum correlation with neighboring stations were used in the regression model to interpolate data for the CSL and MZN unfiltered residual series. For the interpolation of the MZN series, ACA and CSL were used as neighboring stations, whereas for CSL, MZN and Punta Baja (PBA, see Figure 1) were used. Gaps greater than 13 days were found in the original time series, but they were not interpolated. Finally, interpolated time series were filtered using the PL64 filter. Correlation, spectral, and cross-spectral functions were estimated before and after the larger gap interpolation. It was verified that these statistics were not significantly altered by the interpolation methods. For example, maximum-lagged correlation between MZN and CSL, during the available common period, was the same before and after the interpolation (0.57).

Wind data from 2002 to 2006 were obtained from the Cross-Calibrated Multiplatform (CCMP) database [*Atlas et al*., 2011]. The resultant database has a regular grid with a $0.25^\circ \times 0.25^\circ$ resolution. Only data inside the GC, from the northern part of Angel de la Guarda Island (see Figure 1) to the mouth of the gulf, were used. A comparison of the CCMP data with an observed wind time series was performed as a check on the reanalysis winds. An observed wind series spanning November 2003 to December 2006 was available at Cabo Pulmo near CSL (see Figure 1). The complex correlation coefficient [*Kundu*, 1976] between both vector time series had a magnitude of 0.85 and a phase of 1.8°. The phase gives the average rotation needed to align both vector time series. Wind stress was estimated from the 6 hourly winds using the *Large and Pond* [1981] formula. The annual and semiannual harmonics accounted for an average of 26% of the along-gulf component (127° counterclockwise from east) of the wind stress, and they were removed. The 6 hourly, along-gulf component of the wind stress (positive toward the head of the gulf) was filtered with a Lanczos filter with a half-power point at a period of 1.8 days, which is very close to the 1.6 days half-power point of the PL64 filter used for the hourly data.

Moored currents, temperature, and coastal subsurface pressure were obtained from two different observational projects. As part of the UMBRALES project (2002–2006), moorings with a bottom-mounted ADCP

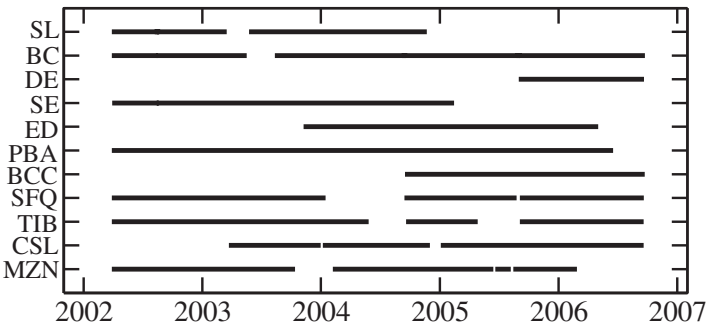

Figure 2. Bars showing the measurement periods for each mooring and coastal subsurface pressure stations. The abbreviation for each station is listed on the left where two-letter stations are current and deep (≥400 m) near-bottom temperature moorings and three-letter stations are for SsP. Current and temperature records have the same length.

were deployed at the four main sills of the northern GC (Figure 1): San Lorenzo sill (SL, ∼400 m depth), San Esteban sill (SE, ∼600 m depth), Delfin sill (DE, ∼400 m depth), and Ballenas Channel sill (BC, ∼600 m depth). All ADCPs were configured with a 10 m vertical resolution and measured currents to about 50 m from the surface. Some of the moorings had an additional Sontek MD Argonaut or AANDERAA RCM9 and a SBE SM37 Microcat, below the ADCP at about 8 m above the bottom. At the SE, BC and DE moorings, 75 kHz ADCP's were installed with a sampling interval (Δt) of 30 min while a 150 kHz ADCP was installed at SL sill with a Δt of 1 h. Not all moorings were installed simultaneously and Figure 2 shows the different periods when moorings were deployed. Some of the observations from these moorings are described in *LCA* and *LCG*. In addition to the deep moorings, pressure and temperature sensors (SBE26) were installed near the coast to measure SsP at depths ranging from 7 to 20 m. These sensors were installed at Ballenas Channel Coast (BCC), Tiburón Island (TIB), San Francisquito (SFQ), and Punta Baja (PBA) on the western coast of the peninsula. The locations of the SsP measurements are shown in Figure 1 and dates of data collection are shown in Figure 2.

A mooring was also deployed at about 180 m depth at the mouth of the GC on the mainland side (Figure 1), as part of the oceanographic campaign PESCAR (PEgasus in the Sea of Cortes Area). This mooring, referred to as El Dorado (ED), was deployed on five occasions between November 2003 and May 2006 (Figure 2). ED included a near-bottom 250 kHz Sontek ADCP at ∼115 m depth with a vertical resolution of 4 m, and three Microcats at 40, 80, and 120 m. Only the deepest Microcat was used in this study. The Δt for the instruments on the ED moorings was 15 min. At each location, moorings were deployed at slightly different depths so currents were linearly interpolated to common depths. Gaps between each ED mooring lasted less than 10 h and they were bridged using linear interpolation.

SsP data from the pressure sensors were processed in exactly the same manner as the tide-gauge data, except no atmospheric pressure correction and interpolation were required as there were no gaps less than 13 days. Current time series were filtered with the PL64 filter and the currents were rotated to the mean angle (in the vertical) of the major principal axis at each location. Depth variation of the orientation of the major axis at each location was on the order of 10°, except at the DE mooring, where near-surface currents showed more variability. However, rotated currents at all locations proved to be within ±15° from 127° counterclockwise from east, which marks the mean axis of the gulf. Therefore, positive (negative) currents are toward the head (mouth) of the gulf.

3. Results

In section 3.1, empirical orthogonal functions of along-gulf currents at the three moorings are shown. Then, SsP observations are described with emphasis on the relation that existed between MZN and CSL with stations inside the gulf. Given the previous evidence of CTWs propagating into the GC as mentioned in the introduction, MZN was used as a proxy for CTW propagation into the gulf. In sections 3.3 and 3.4, the relationship between SsP at MZN and currents, near-bottom temperature, and transport in the GC are analyzed. Finally, the relationship between the wind stress and currents is investigated.

3.1. Empirical Orthogonal Functions of Currents

Empirical orthogonal functions (EOFs) of the along-gulf currents were computed for all available observations at the SL and BC moorings. Currents measured at these moorings, which were

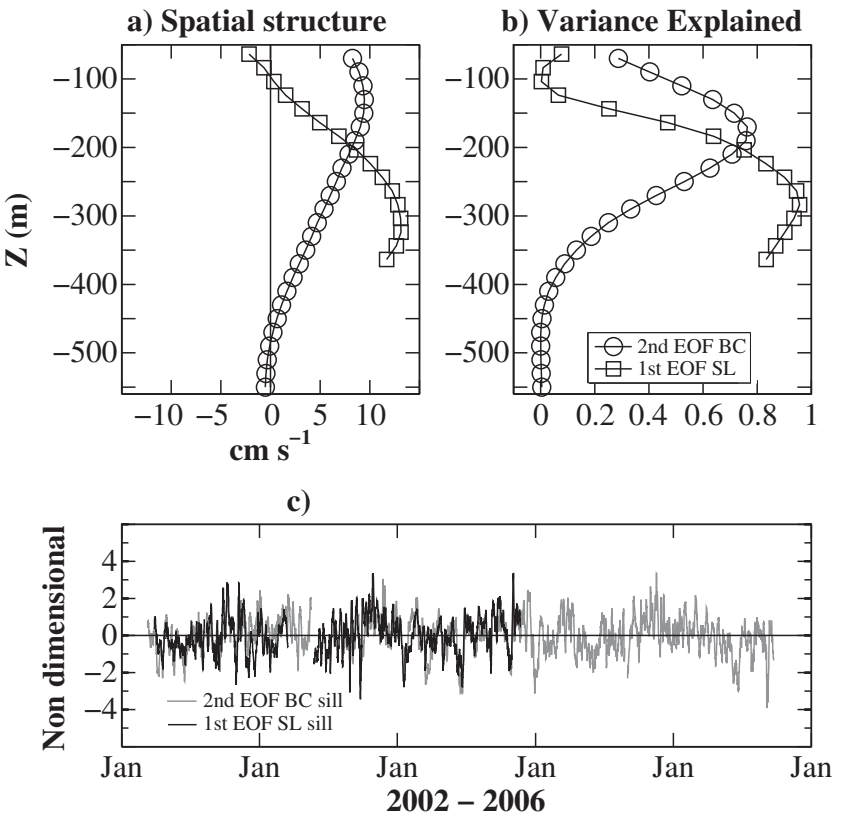

Figure 3. Empirical orthogonal functions of the low-frequency along-gulf currents at the BC (circle) and SL (square) sills. (a) Spatial structure of the first and second modes of the currents at the SL and BC sills, respectively. (b) Variance explained by each mode as a function of depth. (c) Time series associated with the empirical modes. The black and gray lines correspond to the first and second modes at the SL and BC sills, respectively. The EOFs were computed using all available data at each mooring.

representative of the currents in the NGC, had higher correlations with SsP at MZN than the other two moorings at DE and SE (see section 3.3). The spatial structure, time series and the variance explained for the SL and BC moorings first and second mode, respectively, are shown in Figure 3. The first mode for the SL sill explained 75% of the total variance and was dominated by the near-bottom currents where the maximum values of the spatial structure and variance explained were located at ∼300 m. For positive principal component values, this mode is associated with an intensification of the strong near-bottom inflow of relatively fresh and cold water toward the head of the gulf [*LCG*]. The first mode at the BC (not shown) explained 45% of the total variance and was also dominated by near-bottom currents. The time variation of this mode had a lower correlation than the second mode with the first mode at the SL sill (Table 1). The second mode at BC explained ∼33% of the total variance with maximum values of ∼75% between 150 and 200 m whereas the largest mean and fluctuating velocities were located between 100 and 150 m [*LCA*]. This second mode at BC and the first mode at SL had a relatively high correlation (0.67), such that near-bottom current fluctuations toward the head of the gulf at the SL sill were related to near-surface current anomalies in the same direction at the BC sill (see Table 1).

The first mode at the ED mooring explained 83% of the total variance and the spatial structure (not shown) was quasibarotropic with fluctuations having the same sign at all depths (19–111 m). Figure 4 shows the time series for the first EOF of currents at ED and SL sill. The first mode time series of ED and SL (Figure 4) had a negative correlation of −0.49 at a lag of −3.3 days indicating that current fluctuations toward the head of the gulf at the ED mooring led near-bottom current fluctuations toward the mouth of the gulf at the SL mooring. Correlation between the first ED and second BC modes was −0.43 (lag of −6.3 days) such that currents toward the head of the gulf at ED led near-surface currents toward the mouth at the BC sill (Table 1).

Table 1. Maximum-Lagged Correlations for Time Series Described in the First Two Columns[a]

Variable 1	Variable 2	Common Period	Maximum-Lagged Correlation[b]	Lag Days[c]
1st Mode SL	1st Mode BC	28 May 2002 to 21 Nov 2004	0.47	−3.8
	2nd Mode BC		0.67	0.3
1st Mode ED	1st Mode SL	8 Nov 2003 to 21 Nov 2004	−0.49	−3.3
	2nd Mode BC		−0.43	−6.3
MZN	1st Mode ED	8 Nov 2003 to 26 Feb 2006	0.50	−2.5
	1st Mode SL	28 Mar 2002 to 21 Nov 2004	−0.45	−6.0
	2nd Mode BC	10 Mar 2002 to 26 Feb 2006	−0.35	−7.2
MZN	Temp ED	8 Nov 2003 to 2 May 2006	0.61	−3.3
	Temp SL sill	28 Mar 2002 to 21 Nov 2004	0.59	−6.3
	Temp SE sill	29 Mar 2002 to 13 Feb 2005	0.44	−6.1
	Temp BC sill	10 Mar 2002 to 26 Feb 2006	0.68	−24.1
MZN	Q SL sill	28 Mar 2002 to 21 Nov 2004	−0.43	−5.9
*SL sill 364	Temp SL sill		−0.77	−0.4
Q SL sill			−0.59	−1.0
1st Mode τ_r	Q SL sill		−0.35	−2.5
	V_{geo}	15 Mar 2002 to 19 Sep 2006	0.34	−2.0
MZN		15 Mar 2002 to 26 Feb 2006	0.40	−5.9
Q SL sill		28 Mar 2002 to 16 Nov 2004	−0.65	0.2

[a]Modes refer to EOFs of low-frequency along-gulf currents described in section 3.1. MZN refers to SsP at Manzanillo, and the two letter acronyms (SL, BC, ED, and SE) refer to moorings described in section 2. The acronyms Temp, Q, τ_r, and V_{geo} refer to near-bottom temperature, bottom transport, first EOF mode of along-gulf wind stress, and geostrophic velocity fluctuations averaged across the gulf, respectively. "*" currents at SL mooring measured at 364 m.
[b]All values are significant at the 95% confidence level.
[c]Negative lags mean variable 1 led variable 2.

3.2. Subsurface Pressure Data

Variance-preserving, autospectral density functions were estimated for the SsP records using the Welch-periodogram method in which the time series were divided into equal segments of 120 days (Figure 5). Periodograms were obtained with zero overlapping and multiplied by a Hanning window. One advantage of using the Welch method is that it allows estimating spectra of time series with gaps provided that time series have segments of the appropriate length without gaps. Not all spectra were estimated over the same periods, but periods were chosen for maximum overlap between the different locations.

MZN had most of the energy in the 40–120 day band (intraseasonal band), and there was a second peak with less energy in the 10–20 day band (synoptic band). Inside the GC, the energy in the intraseasonal band dropped substantially for the 40–120 day periods. At TIB (Figure 5b), two different periods were used to estimate the spectra. The period showing larger energies includes the relatively strong 2002–2003 El Niño, according to the Oceanic Niño Index (www.cpc.ncep.noaa.gov/products/analysis_monitoring/ensostuff/ensoyears.shtml). Larger instraseasonal energy in CTWs during El Niño years was consistent with the results of *Spillane et al.* [1987]. Intraseasonal energy dropped significantly on the Baja California side of the GC (SFQ) and it dropped even more on the northern GC (BCC), where energy in the intraseasonal band was the lowest and, similar to CSL at the southern tip of Baja California. The energy in the synoptic band also decreased by half inside the GC. In addition to MZN, the synoptic energy remained relatively high at CSL.

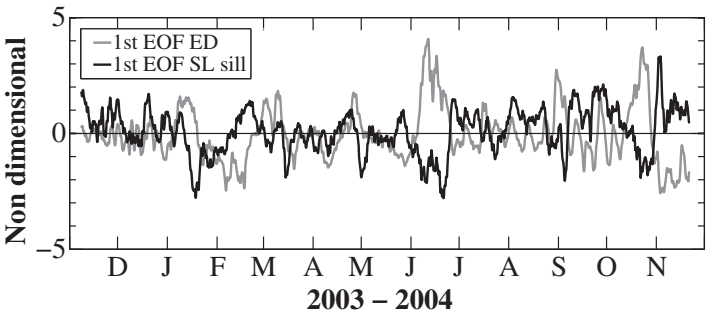

Figure 4. Time series associated with the first empirical modes for the low-frequency along-gulf currents at the ED (gray) mooring and the SL sill (black). The simultaneous period is from November 2003 to November 2004.

Correlation functions between stations within the sill zone and MZN and CSL were estimated in order to study the propagation of SsP anomalies (Figure 6). Correlation with a station on the Pacific side of the peninsula (PBA) was also included to determine if signals, propagating through

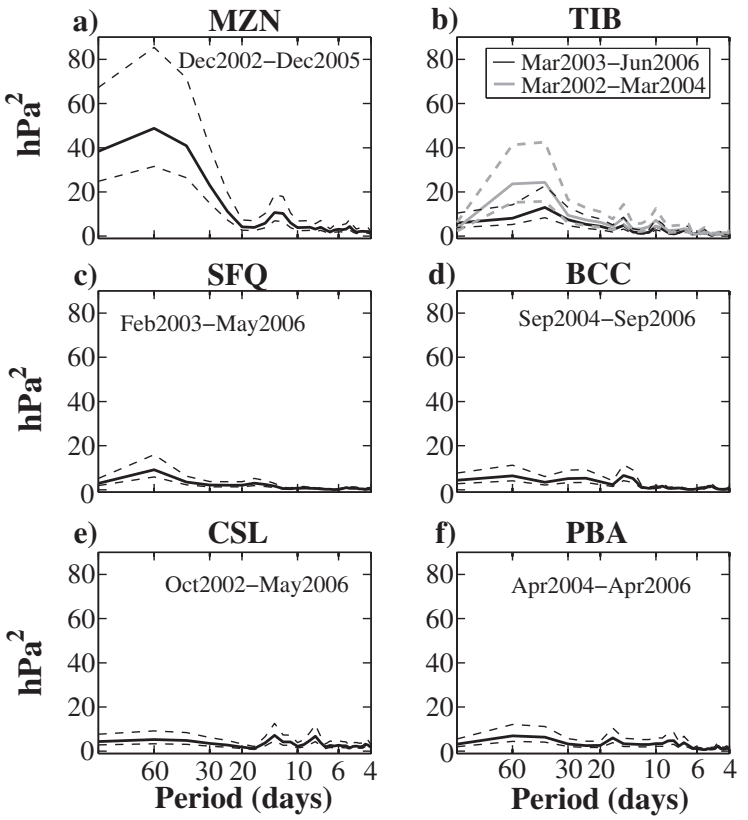

Figure 5. Variance-preserving spectra of the SsP records. Estimates were calculated using 32 degrees of freedom. Dashed line shows the 95% confidence limits for each estimate. The period used for calculating the autospectral density for each station is indicated.

MZN and CSL, were able to reach that station. The correlation functions using MZN as a base station are shown in Figure 6a. The common period for all stations was 17 months. Correlation functions between MZN and TIB, SFQ and BCC indicated one maximum positive correlation where a positive SsP anomaly at MZN led those stations in the sill zone by 5–7 days, consistent with the propagation of CTW toward the GC with a phase speed of 190–270 km d^{-1}, similar to those found by other authors [e.g., *Christensen et al*., 1983; *Enfield and Allen*, 1983; *Spillane et al*., 1987; *Merrifield and Winant*, 1989]. The significant correlation between MZN and BCC indicated that the effect of CTWs could reach the Northern Gulf beyond the sill zone. The correlation function between MZN and CSL showed a double maximum, and the first maximum was located at almost zero lag (−12 h) and the second occurred at −10 days (MZN leading CSL). The first maximum could indicate a possible transfer of energy of the CTWs across the mouth of the gulf or a possible forcing due to tropical storms, which often travel northward along the tropical Mexican Pacific coast [*Enfield and Allen*, 1983]. On the other hand, the second maximum was consistent with CTWs propagating from MZN, around the GC and then reaching the tip of the peninsula at CSL [*Martínez and Allen*, 2004a, 2004b]. For PBA, the maximum-lagged correlation was located in a wide band between −15 and −10 days.

The correlation functions between CSL (as the base station) and the other stations were estimated for a common 22 month period (Figure 6b). The correlation function between CSL and TIB also showed two maxima. The smaller maximum at CSL led TIB by ∼3 days, consistent with energy being transferred across the mouth of the gulf. The larger maximum was broader and centered around 6 days with TIB leading CSL, consistent with CTW energy that travels around the gulf. Also, two maxima can be seen in the correlation function between CSL and PBA, with CSL leading PBA by ∼4 days (largest maximum) and by ∼12 days (smaller maximum). Again, these two maxima were consistent with energy being transferred across the mouth of the gulf (larger maximum, smaller lag) and energy propagating around the gulf (smaller maximum, larger lag). In both cases, the energy appears capable of propagating poleward along the Pacific coast of Baja California [*Spillane et al*., 1987]. The correlation functions with BCC and SFQ showed the maximum correlation

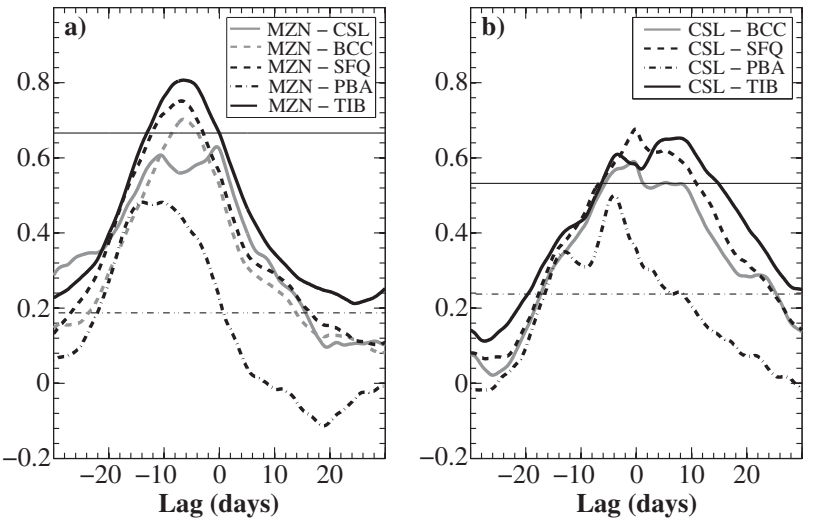

Figure 6. (a) Correlation functions between MZN and different stations inside the gulf and with PBA for a common period from September 2004 to February 2006. (b) Correlation functions between CSL and different stations inside the gulf and with PBA for a common period from September 2004 to July 2006. The horizontal thick and dashed lines indicate the 95% significance level for the correlation functions with TIB and PBA, respectively. Negative lag indicates that the first station (MZN or CSL) leads the second station.

at zero lag. This was somewhat puzzling since it would indicate simultaneous events between these two stations and CSL. However, other explanations are possible and will be discussed in the next section.

The coherence spectra between MZN and remote SsP stations are shown in Figure 7. For all stations, the highest significant coherences were found for periods of 30–60 days. The phase between MZN and CSL (Figure 7a) was between 2 and 3.5 days (MZN leads CSL). Note that this phase was smaller than the phase of MZN-TIB (3–5 days, MZN leading TIB) for the same period band. The phase between MZN-TIB (Figure 7b) was consistent with the lag obtained by the corresponding correlation function. There was a small, albeit significant coherence for MZN-BCC (Figure 7c) with a phase of ∼5 days in the 30–60 day period. This is evidence that at least some energy of intraseasonal CTWs reached the Northern Gulf. For MZN-SFQ (Figure 7d), the phase spectrum showed that MZN led SFQ by ∼5 days. The lack of coherence at synoptic frequencies was due to the fact that such coherences were observed during the summer storm season [*Enfield and Allen*, 1983; *Merrifield*, 1992] and the records used in Figures 7b and 7d lack two of the four possible summers. Significant coherences at synoptic frequencies were obtained for the available MZN-TIB and MZN-SFQ summer records (not shown). The coherence and phase spectra of CSL-SFQ (Figure 7e) and CSL-BCC (Figure 7f) showed significant coherences for the 60 day band with almost zero phases, which is consistent with the lag of the corresponding correlation functions.

3.3. Relationship Between MZN and Currents

Maximum-lagged correlations between MZN and the time series of current EOFs are summarized in Table 1. At the SL sill, the negative correlation implied that a positive (negative) SsP anomaly propagating into the GC would reduce (increase) the mean, near-bottom flow toward the head of the gulf that has been found to be part of the vigorous exchange with the NGC [*LCA; LCG*]. At the BC sill, only the second mode was significantly correlated with MZN such that positive SsP anomalies led near-surface currents fluctuations toward the mouth. In summary, these correlations showed that positive SsP (downwelling of the thermocline for baroclinic waves) associated with CTW propagating into the gulf generated current fluctuations in the opposite sense to that of the mean flow near the surface (bottom) at the BC (SL) sill [*LCA*]. Note that the correlation between MZN and the EOF at the SL sill was larger than the corresponding one with the SE sill, although this latter sill is closer to the eastern coast of the gulf where CTWs first arrive to the complex zone of the southern sills (not shown). This may be related to stronger dissipation and mixing at the SE sill where the strongest tidal currents are found [*LCA*], but also to the different character of the near-bottom transport toward the head of the gulf at the SE sill, as discussed in the last paragraph of the next section.

Profiles of squared coherences between MZN and currents at the ED and SL sill are shown in Figure 8. Significant coherences were found for 20–60 day periods, at all depths for ED (Figure 8a), and for 30–60 day

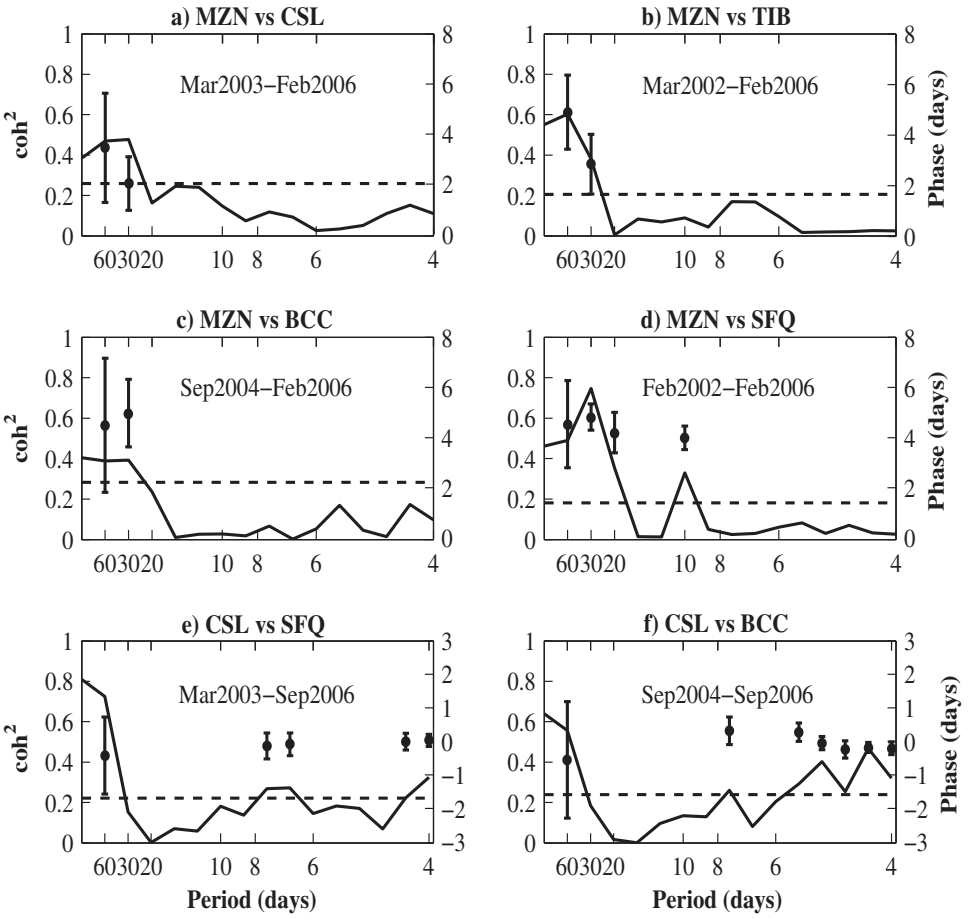

Figure 7. Coherence (solid) and phase in days (dots) for SsP stations between MZN and (a) CSL, (b) TIB, (c) BCC, and (d) SFQ; and between CSL and (e) SFQ and (f) BCC. The horizontal dashed line indicates the 95% significance level for squared coherences. Positive phase indicates the first station (MZN or CSL) leads the second station. Error bars indicate the 95% confidence range for phase estimates when the coherence exceeded the 95% significance level. Common period for each estimate is indicated.

periods only below 150 m depth at SL sill (Figure 8c). At SL sill, the highest coherences were found for currents close to the bottom at the 12, 30, and 60 day periods, which was consistent with the corresponding correlation with the bottom-intensified EOF mode shown in Table 1. Phase profiles at ED (Figure 8b) for the 20–30 day periods were positive everywhere, such that positive SsP at MZN led currents toward the head of the gulf at ED with phase lags ranging from 0 to 6 days near the surface. Note, however, that there was a variation of phase with depth for the 60 day band consistent with a baroclinic response and/or frictional effects [*Romea and Allen*, 1984]. At the SL sill, phase lags (Figure 8d) for the highest coherence periods, were such that SsP at MZN led current fluctuations toward the mouth of the gulf (i.e., negative phases plus 180°) with lags between 2.4 and 7 days, in agreement with the lag of the corresponding correlation with the first EOF mode (Table 1). There was also significant coherence at both locations for the synoptic frequency band. At the BC sill, coherences with MZN SsP were low and only barely significant close to the surface and for periods of 60 days. Phases for this band were around 5 days with MZN leading current fluctuations toward the mouth of the gulf (not shown).

3.4. Near-Bottom Temperature and Transport

Correlations of temperature with SsP at MZN are shown in Table 1. All temperature records are essentially at the bottom (∼10 m from the bottom) in at least 400 m of water, except for the temperature at ED, which was at ∼110 m in 150 m of water. Annual and semiannual harmonics were removed from the temperature records. All correlations were relatively good ($r \sim 0.5$–0.6) and positive, which was consistent with a baroclinic response to MZN SsP propagating into the gulf (i.e., a positive SsP is associated with a lowering of the isotherms in a baroclinic wave). This was also consistent with the correlations and coherences of MZN SsP

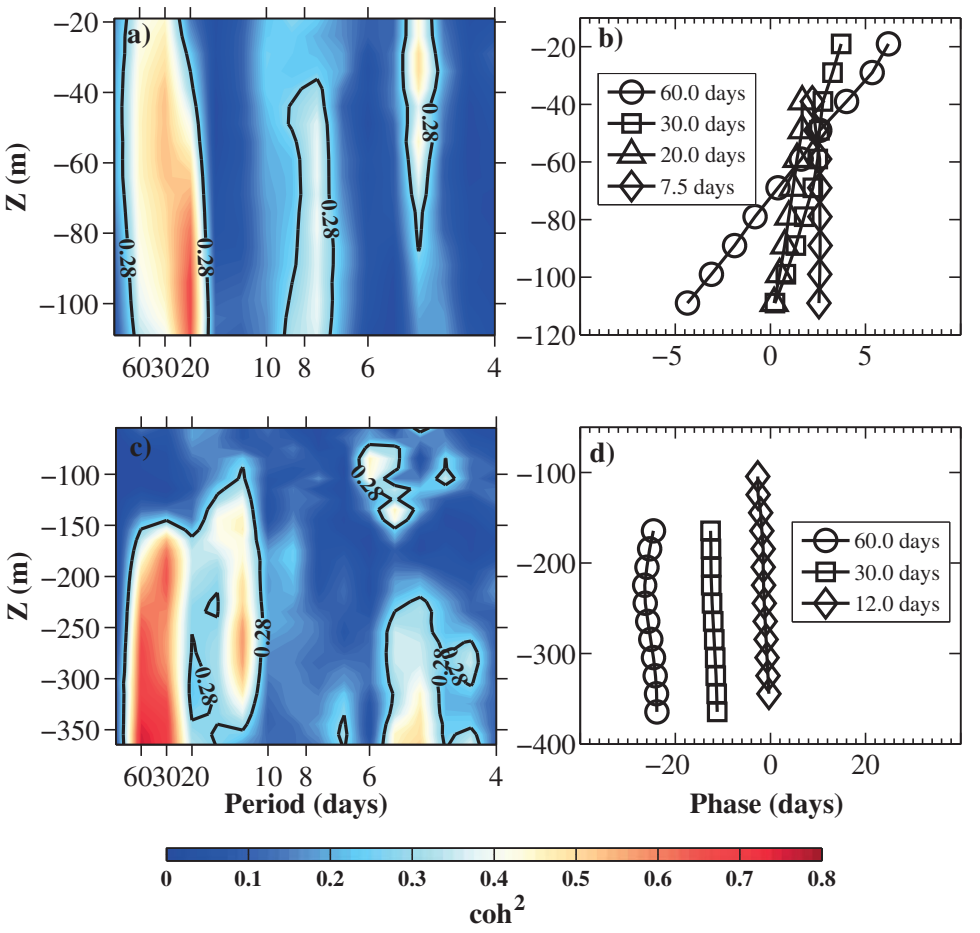

Figure 8. (left) Coherence squared and (right) vertical profiles of phase in days between SsP at MZN and along-gulf currents at (a and b) ED mooring and (c and d) the SL sill. Color bar indicates the coherence squared and the thick contour shows the 95% significance level. Phase profiles are only shown for some selected squared coherences that are above the significance level. Positive phase indicates that MZN leads currents toward the head of the gulf. Phase symbols are placed at every other data point.

with currents at the SL sill, since a weakening of the mean, near-bottom flow toward the head of the gulf was associated with warmer water entering Ballenas Channel over the SL sill as evidenced by the negative correlation between near-bottom temperature and near-bottom currents and transport at that location (see Table 1). Negative lags showed SsP at MZN led warmer temperatures at ED, as well as at the SL and BC sills by lags consistent with propagation of CTWs. However, at the BC sill the lag is too large (−24 days). A possible explanation for this lag will be discussed in the next section. The coherence between MZN and near-bottom temperature at the SL sill is shown in Figure 9a. The highest coherence was for periods of 60–30 days with MZN leading a positive anomaly of temperature at SL by ∼4 days.

The SL and SE sills constitute the locations where deep inflow enters the NGC from the southern gulf and the Pacific Ocean [*LCA; LCG*]. Given the significant correlations and coherences between MZN SsP and near-bottom currents and temperature at the SL sill, it was important to obtain correlations and coherences with bottom transport at this sill of the NGC. At the SL sill, there is an overflow and the transport is mainly due to the mean flow [*LCA*]. The 18 month long transport time series estimated by *LCG* was augmented by the transport estimated from the first two moorings, spanning almost a year. This 30 month long time series (with a gap of about 2 months) was used for the correlation and coherence with MZN and other variables described in the following section. The mean transport for the extended time series was estimated to be 0.07 ± 0.01 Sv.

Transport at the SL sill was negatively correlated with SsP at MZN, such that a positive anomaly at MZN led by ∼6 days a reduction of the bottom transport toward the head of the gulf (Table 1). Coherence and phase

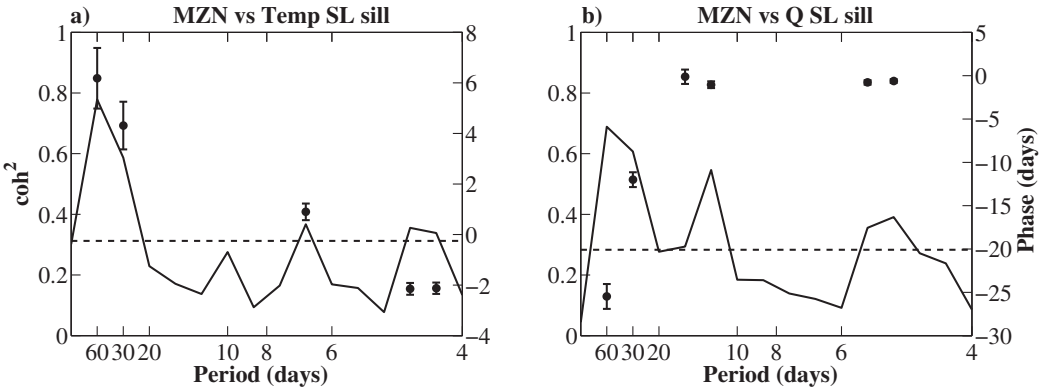

Figure 9. Coherence (solid) and phase in days (dots) between SsP at MZN and (a) near-bottom (~400 m) temperature anomalies at the SL sill and (b) bottom transport anomalies at the SL sill. The horizontal dashed line indicates the 95% significance level for squared coherence. Positive phase indicates MZN leads temperature and positive transport (toward the head). Error bars indicate the 95% confidence range for phase estimates for which the coherence exceeded the 95% significance level. Common period is from 29 March 2002 to 21 November 2004.

between MZN SsP and SL sill bottom transport (Figure 9b) showed, as in the case of temperature, higher coherence for intraseasonal periods. The phase indicated that a positive anomaly at MZN led negative transport fluctuations toward the mouth of the gulf by about 5 days for the 30 and 60 day periods. Bottom transport and near-bottom currents were negatively correlated with near-bottom temperature at the SL sill (Table 1). In turn, near-bottom temperatures were well correlated (0.89) with near-bottom salinities [*LCG*]. Therefore, lagged correlations and coherence between MZN and along-gulf currents, near-bottom temperature and bottom transport showed that downwelling (upwelling) CTWs reduced (increased) the fresher and colder subsurface, subtropical water from the Pacific Ocean that overflows into the Ballenas Channel through the SL sill. For a more quantitative estimation of this relationship, transfer function between MZN and the bottom transport at the SL sill was estimated (Figure 10). Intraseasonal waves (30 and 60 day periods) changed the transport by about 10% of the mean transport for each cm of sea level that propagates from MZN and reached the sill zone in the NGC.

The transports at the DE and SE sills were compared with SsP at MZN. For DE, the correlation was not significant, possibly due to a short 6 month common period (September 2005 to February 2006). At the SE sill, the maximum correlation coefficient was −0.28, which was marginally significant (−0.17) at zero lag. At the SE sill the transport is not due to the mean flow but to a rectification of the near-bottom transport by the tidal currents. The Eulerian mean flow is actually toward the mouth of the gulf in the opposite direction to the near-bottom, volume transport, which is toward the head of the gulf [*LCA*]. Furthermore, at the SE sill the energy at the 15 day band (not shown) appears to be somewhat larger than the energy at the same band on the other sills. The energy at the 15 day band is most likely due to nonlinear effects associated with tidal currents.

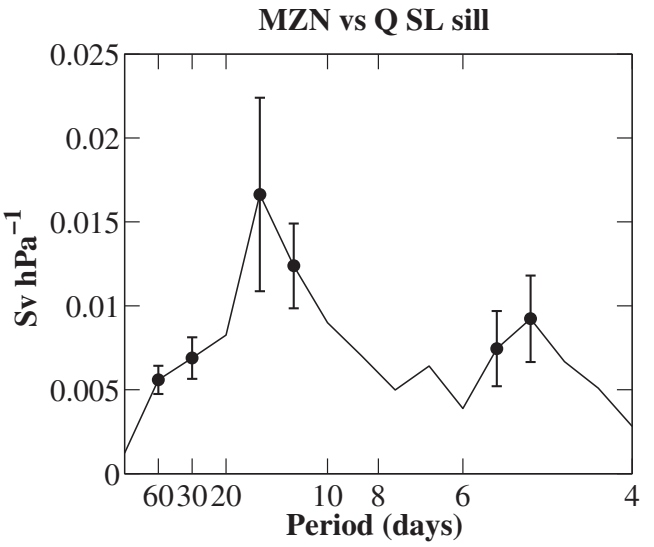

Figure 10. Magnitude of transfer function between SsP at MZN (in hPa) and bottom transport at SL sill (in Sv). Dots show values where squared coherence was above 95% significance level (see Figure 9b). Error bars indicate the 95% confidence range for the transfer function and were calculated only for those frequencies in which squared coherence was significant, according to *Bendat and Piersol* [1986]. Common period is the same as in Figure 9.

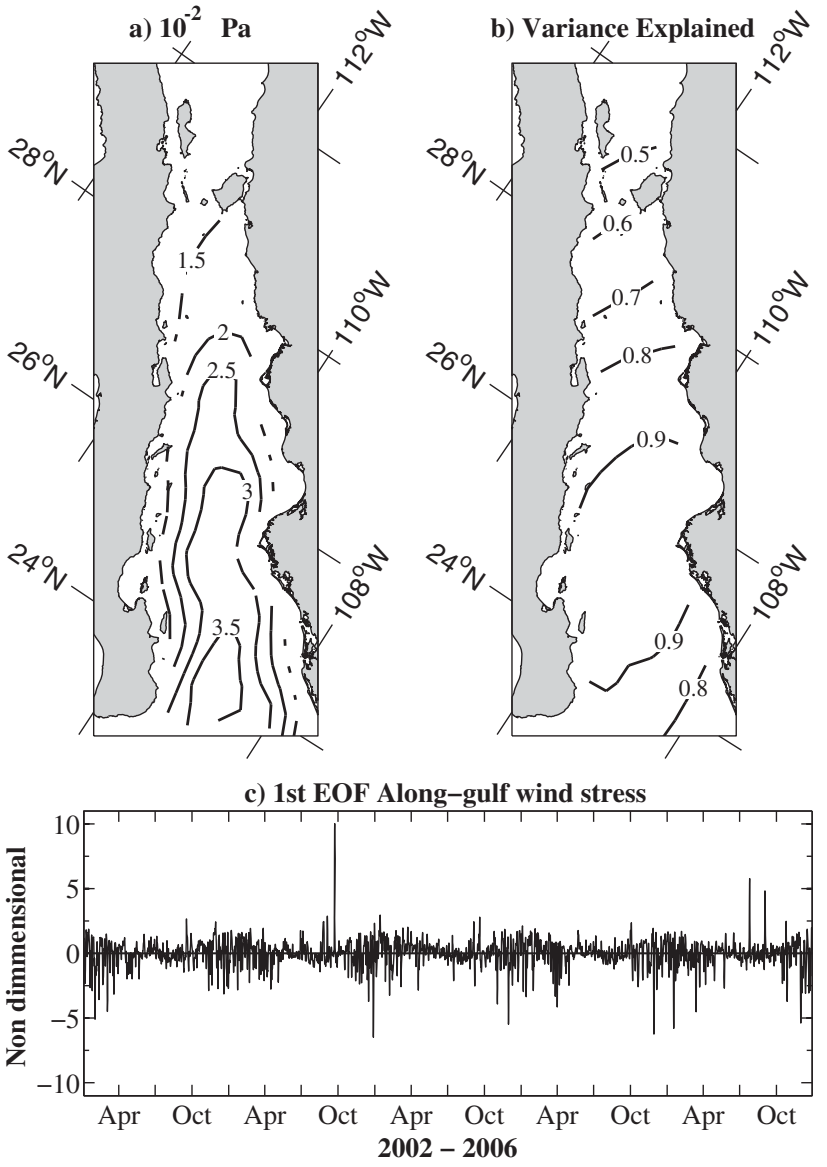

Figure 11. First Empirical Orthogonal Function (EOF) of 6 hourly along-gulf wind stress in the Gulf of California from CCMP wind data from January 2002 to December 2006. (a) Spatial structure of the first mode. (b) Spatial structure of the proportion of variance explained by the first mode. (c) Time variability associated with the first mode.

3.5. Wind Stress and Currents

In order to explore the possible effects of local wind stress on the currents and bottom transport in the GC, EOFs of the along-gulf wind stress were calculated (Figure 11). The first EOF accounted for 86% of the total variance without the annual and semiannual cycles. The spatial distribution of the first eigenvector (Figure 11a) and local variance (Figure 11b) showed values that increased from the sill zone toward the mouth of the gulf. The temporal variation of the first mode (Figure 11c) showed high variability. In addition, to further investigate the effect of CTWs and wind stress on the exchange through the surface and near the bottom, geostrophic velocity fluctuations were estimated between TIB and SFQ by using the difference between the corresponding SsP records and the distance between both stations (~57 km). Note that the difference in SsP between these two stations was proportional to the surface geostrophic velocity fluctuations *averaged across the gulf* (V_{geo}). TIB minus SFQ, was calculated so that positive surface geostrophic current fluctuations flow toward the head of the gulf (see dotted line in Figure 1).

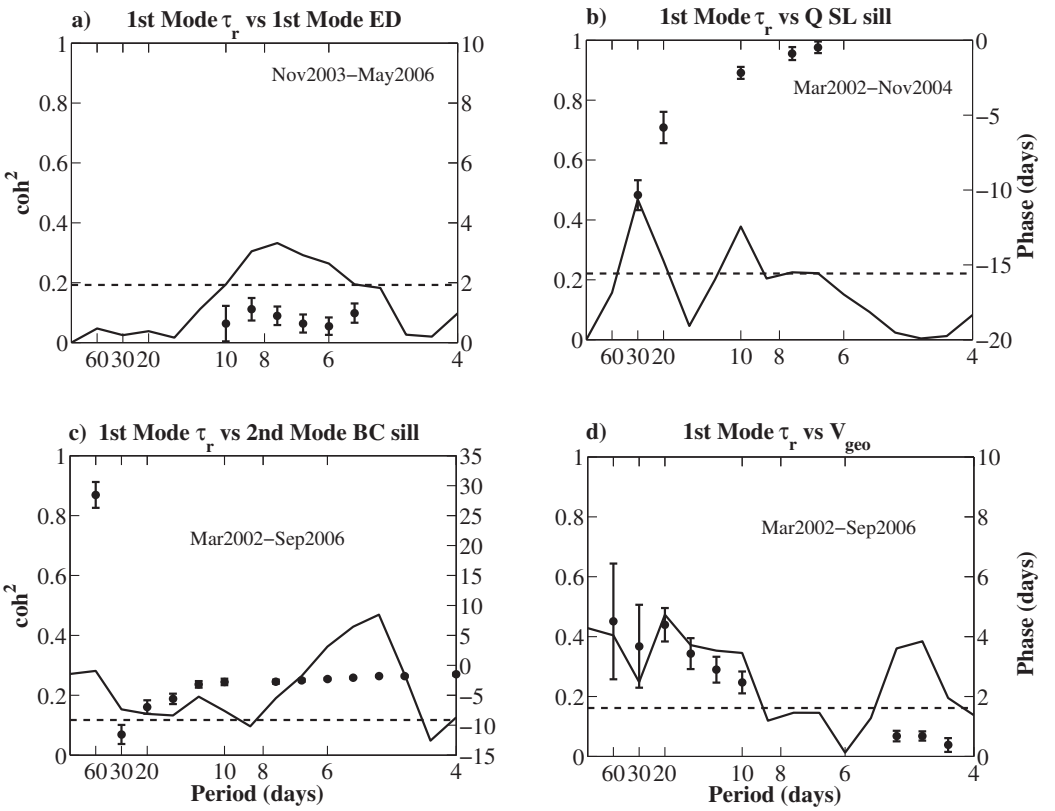

Figure 12. Coherence (solid) and phase in days (dots) between the first EOF of wind stress and (a) first EOF mode of currents at ED, (b) near-bottom transport at SL sill, (c) second EOF mode of currents at BC, and (d) surface geostrophic velocity. Positive phase indicates wind stress toward the head leads currents and transport in the same direction. Error bars indicate the 95% confidence range for phase estimates for which the coherence exceeded the 95% significance level. Common period for each case is indicated.

The correlations between wind stress and bottom transport and surface geostrophic velocity were low, but statistically significant, at similar lags of about 2 days (see Table 1). The positive correlation with surface geostrophic velocity was consistent with Ekman transport producing higher sea level on the mainland coast, whereas the negative correlation with bottom transport was consistent with the exchange pattern of the NGC: the bottom and surface layer fluctuations responding in opposite directions.

Coherence functions between the first EOF mode of wind stress and currents and transport are plotted in Figure 12. Coherence values were generally low, albeit significant, at certain frequency bands. At ED (Figure 12a), coherences were only significant at the synoptic frequency band with wind leading currents by lags on the order of 1 day. In contrast, at the SL sill (Figure 12b) the near-bottom transport was most coherent with wind stress at 20 and 30 day periods, with wind leading transport toward the mouth by about 5 days (i.e., phases in Figure 12b plus 180°). At the BC sill (Figure 12c), the near-surface intensified second EOF mode had the highest coherences at periods smaller than 6 days, with wind leading currents toward the mouth by about 1 day. Note that, for the 60 day band, the currents appeared to be almost 180° out of phase with the wind. However, with the error bars for the phase, this could also be interpreted as a negative phase just as the other phases shown in which wind stress toward the head led currents toward the mouth by a few days. Wind stress was coherent with the surface geostrophic velocities over a 10–60 day period with wind, blowing toward the head of the gulf, leading velocity fluctuations in the same direction by 2–5 days (Figure 12d). Note that the phases between wind and bottom transport, and wind and surface geostrophic velocities have opposite signs, which is consistent with the exchange pattern of the NGC.

There was also a relatively high negative correlation ($r = -0.65$) between bottom transport at the SL sill and surface geostrophic velocity anomalies at almost zero lag (Table 1). This was consistent with the two-layer exchange of the NGC first proposed by *Bray* [1988] and *Lavín and Organista* [1988]. The mean of the near-bottom (lower-layer) transport is toward the head of the gulf [*LCA*], and the negative correlation showed

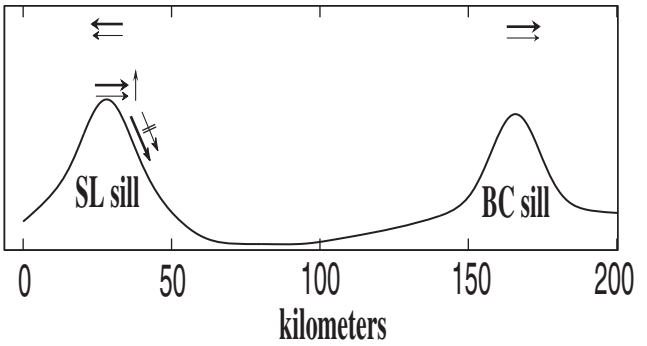

Figure 13. Simplified picture of the mean flow (thick arrows) and current fluctuations (thin arrows) induced by SsP depression (upwelling) CTWs and down-gulf winds at the sills of Ballenas Channel. Current fluctuations by SsP elevation (downwelling) CTWs and up-gulf winds are the thin arrows reversed. Sloping arrows correspond to the mean overflow (thick arrow) and the fluctuating contribution (thin arrow with two crossing lines) due to the near-bottom inflow by upwelling CTWs and down-gulf winds. This latter arrow does not reverse because the fluctuating near-bottom inflow is denser than the outflow and feeds the overflow.

that fluctuations of the bottom transport are essentially 180° out of phase with surface geostrophic velocity fluctuations averaged across the gulf. Finally, the maximum-lagged correlation between MZN SsP and surface geostrophic velocity anomalies was 0.4 (Table 1) with MZN leading geostrophic velocities toward the head by the same lag as that between MZN and the near-bottom transport at the SL sill. This correlation showed that CTWs, propagating from MZN, generated geostrophic velocity fluctuations at the sill zone that were roughly in phase (i.e., for intraseasonal CTWs) with positive SsP at MZN. This is to be expected for long CTWs, which have an approximate geostrophic alongshore momentum balance. In summary, as shown schematically in Figure 13, along-gulf wind stress fluctuations toward the head (mouth) of the gulf and positive (negative) SsP CTWs tend to reduce (increase) the exchange with the Northern Gulf, for the upper and lower layers.

The first EOF of the wind stress curl inside the gulf was also obtained. This mode explained 62% of the variance and was positive (negative) on the continental (peninsular) side of the gulf (not shown). This mode showed correlations (albeit with opposite signs) and lags to bottom transport (0.35) and V_{geo} (−0.31) similar to the corresponding correlations with the wind stress. However, it is possible that this reflected the almost perfect negative correlation (−0.97) at zero lag between the wind stress and wind stress curl. This was also reflected in an almost perfect coherence with an 180° phase difference at all frequency bands between these two series (not shown).

4. Discussion and Concluding Remarks

Spectra of SsP were consistent with a strong dissipation (either by bottom friction and/or by scattering to higher modes) of the intraseasonal energy at the mid-riff islands that constitute the entrance to the NGC. Energy decreased significantly for stations on the western and northern parts of the gulf, as well as on the Pacific side of the peninsula, but was somewhat larger at the TIB station, located on the eastern side of the entrance to the NGC (Figure 5). On the other hand, cross-correlation functions (Figure 6a) and coherence functions (Figure 7) show that energy, propagating from the Pacific Ocean, reached the northernmost gulf as evidenced by the relatively high correlation (∼0.7) between MZN and BCC. Lags and phases between MZN and BCC (Figures 6a and 7c) were the same as the phases and lags found for MZN-TIB (Figure 7b) and MZN-SFQ (Figure 7d) and they were more consistent with the rapid propagation found by *Martínez and Allen* [2004a] or with the effect of CTW on the exchange flow of the NGC as discussed below.

The double-maxima correlation functions (MZN-CSL, CSL-TIB, and CSL-PBA in Figure 6) and the smaller phases of the intraseasonal band between MZN and CSL, as compared to the ones between MZN and the stations inside the gulf (Figure 7), were consistent with some of the energy of the waves actually "jumping" the mouth of the gulf and propagating poleward along the western coast of the peninsula. *Spillane et al.* [1987] first pointed out this possibility for the intraseasonal band, although they did not believe that the wave going around the gulf could actually reach the western side of the peninsula. However, in this study, it does present a possibility given the broad maximum (8–14 days) in the correlation between MZN and PBA (Figure 6a) and the double maxima between CSL and PBA and CSL and TIB (Figure 6b). However, correlations between CSL and the first EOF of the ED mooring at the mouth of the gulf were very low (0.23) and marginally significant. Similarly, coherences were not significant in the intraseasonal band. This suggests

that the process of the CTW energy crossing the mouth of the gulf may be more complex and could involve the generation of eddies as CTWs pass capes and other coastline features, as suggested by numerical simulations [*Zamudio et al*., 2007, 2008] and observations [*Lavín et al*., 2013].

The zero lag correlation between CSL and the stations on the western side of the gulf (BCC and SFQ in Figure 6b), together with the almost zero phase lag in the 60 day band (Figures 7e and 7f), was somewhat puzzling since it would indicate simultaneous events at those locations. However, there is an alternative interpretation if two waves are assumed to arrive at CSL: one that transited across the mouth and another that propagated around the gulf, although not necessarily around the head of the gulf, but somehow reflecting at the mid-riff islands where the southern sills are located. The effect of the CTWs on the northernmost sill (BCC SsP and BC mooring) would be through the effect of these waves on the exchange as discussed below. The phases of these two waves would have different signs with respect to the waves inside the gulf, since one arrives earlier at CSL (the one that propagated directly across the mouth). The lags of the correlation and the phase lags of the coherence between CSL and the stations inside the gulf would then be dependent on the relative amplitudes of the two waves arriving at CSL. This idea is further elaborated in Appendix A.

Correlations and coherences between remote SsP at MZN and currents, bottom transport, and near-bottom temperature at the sill zone clearly demonstrate an important effect of CTWs on the fluctuations of the exchange between the northern and southern gulf. SsP elevation (depression) waves would generate surface alongshore-current fluctuations toward the head (mouth) and near-bottom current fluctuations toward the mouth (head) and temperature fluctuations consistent with near-bottom downwelling (upwelling) of the isotherms (see Figure 13). The fact that transport in the bottom layer is concentrated in two narrow sills would explain the fact that correlations and coherences of currents in the SL sill were higher with remote SsP near the bottom than near the surface. CTWs propagating along the mainland coast toward the head of the GC and impinging on Tiburón Island could generate significant near-surface geostrophic currents, which was consistent with the positive lagged correlation between SsP at MZN and surface geostrophic currents (Table 1). This latter current, an average across the gulf, excludes the recirculation currents and eddies that do not contribute to the exchange between the northern and southern gulf. The setup of geostrophic currents will necessarily affect the exchange flows and generate fluctuations of bottom transport in the opposite direction to the surface currents (Figure 13), as evidenced by the relatively high negative correlation between these two variables. The fact that this maximum correlation occurs at almost zero lag is consistent with any of the two layers responding almost instantaneously to fluctuations in the other layer, as required by conservation of mass in the NGC. Since the bottom part of the exchange was concentrated in just two sills, it is possible that geostrophic currents generated by CTWs in the eastern part of the gulf (e.g., between Tiburón and San Esteban Islands) produced fluctuations in the bottom transport at the SL sill. This scenario would not require CTWs to actually cross the gulf in order to affect the transport fluctuations at the SL sill.

Lags of correlation and phase lags of coherences between MZN and the SsP (BCC) and the currents (BC) in the Northern Gulf were somewhat variable. However, correlation lags of MZN with BCC (Figure 6a) and with the second EOF mode of currents at BC (Table 1) were the same to those found with SsP at TIB and currents at the SL sill. Moreover, phase lags between MZN and TIB as well as MZN and BCC, were similar (Figure 7). These lags, together with the presence of Tiburón Island and two smaller islands, make it unlikely that CTWs actually passed into Tiburon Basin and continued propagating around the Northern Gulf. Therefore, the effect of CTWs on the northernmost BC sill could be related to the effects on the exchange at the southern SL sill. In contrast, the quasibarotropic response of the ED currents to SsP at MZN is interpreted simply as the effect of CTWs propagating through that site, and the variation of phase with depth (Figure 8b) is possibly related to frictional and/or baroclinic effects.

Near-bottom currents at the SL sill and near-surface currents at the BC sill were reasonably correlated (0.67 between the corresponding EOF modes, see Table 1), such that inflow near the bottom through the southern SL sill was correlated with outflow near the surface through its northern BC sill (i.e., currents toward the head of the gulf at both sills). This pattern of circulation in the Ballenas Channel has been previously proposed for the mean flow [*LCA*] and appears to be valid also for the fluctuating flow. The basic idea is that the overflow continuously "fills" the deep part of the BC basin and produces a vigorous upwelling on the order of 5 m d^{-1}, which in turn produces outflow (out of the channel at both ends) of the upwelled water near the surface [*LCA; LCG*]. Therefore, CTWs producing fluctuations in the bottom transport into Ballenas

Channel through its southern (SL) sill will necessarily produce fluctuations in the near-surface outflow through its northern (BC) sill (see Figure 13).

This effect of CTWs on the exchange pattern of the NGC could explain the relatively large lag of 24.1 days between MZN and bottom temperature at the BC sill (Table 1). Relatively cold near-bottom water enters through the SL and SE sills. The flow entering through the SE sill reaches Delfín sill and overflows into Delfín basin [*LCG*]. If both of these flows at the SE and SL sills were reduced and warmer water entered with the arrival of positive SsP from MZN, then there could be a reduction in the amount of cold water transported to the northernmost gulf. Once the water has passed over the sills, it would be transported by advection to the northernmost BC sill, which would explain the much larger lag with temperature at that sill.

The effect of wind fluctuations on the exchange of the NGC appeared similar to that produced by CTWs. The correlation of surface geostrophic velocities with the wind suggests that the latter drives currents in the same sense as the winds, which in turn drives an opposing bottom transport (Table 1 and Figure 13). The lag of the maximum correlation between wind and surface geostrophic velocities is the same as that between wind and bottom transport. On a seasonal time scale, *Bray* [1988] proposed a similar response of the near-surface (∼50 m) geostrophic currents to the wind in the central gulf. Here we have shown that the same response was also present on shorter time scales, and that the surface geostrophic velocities are correlated with the exchange. *Bray* [1988], on the other hand, thought the exchange did not include the surface layer above 50 m, but was instead concentrated in the intermediate and lower layers.

It is also important to point out how baroclinic CTWs and wind fluctuations contribute to the exchange at the SL sill. At the SL sill there is an overflow (thick sloping arrow in Figure 13), which transports dense water ($\Upsilon_\Theta > 26.6$ kg m^{-3}) found to the south of the sill into Ballenas Channel where it sinks to the bottom (1600 m), because it is denser than the deep waters in the channel (see Figure 4 of *LCG*). The effect of SsP depression CTWs and wind fluctuations toward the mouth will increase the lower layer flow of waters with density greater than the one over the 400 m deep SL sill. When SsP elevation CTWs and wind fluctuations toward the head weakens or reverses the overflow over the SL sill, the density of the water associated to these fluctuations will be $\Upsilon_\Theta < 26.6$ kg m^{-3}. The inflows will cool and increase upwelling in Ballenas Channel while the outflows provide direct communication between the channel and San Pedro Martir Basin (to the south) at sill depth (400 m). The presence of the density-driven overflow provides a mechanism by which SsP depression CTWs and wind-induced current surface fluctuations toward the mouth contribute to the mean exchange of the NGC (thin sloping arrow in Figure 13).

Many authors have shown the importance of the Pacific Ocean on the circulation and thermodynamics of the GC on seasonal and longer time scales [e.g., *Baumgartner and Christensen*, 1985; *Castro et al*., 1994; *Ripa*, 1997]. This study has shown that on shorter time scales the effect of the Pacific Ocean is also important in the exchange of the NGC through the propagation of intraseasonal CTWs. Furthermore, the effect of wind also appears to be important in driving the fluctuating part of the exchange on this same time scale through a coupling of the surface layer with the near-bottom transport confined to the narrow sills. Finally, the correlation between surface geostrophic velocities with the bottom transport at one of the sills has shown direct evidence of the exchange in the NGC.

Appendix A

It is a simple exercise to add two simple sinusoidal waves with phases approximating the waves arriving at CSL and a single wave with an intermediate phase representing the wave arriving at the western side of the gulf. For one station on the western side in the NGC (BCC or SFQ), only one wave from the Pacific Ocean arrives with arbitrary amplitude: $\eta_{SFQ}=\cos(\omega t-\phi_3)$, where $\phi_3$is the phase lag for the wave reaching SFQ. The signal at CSL η_{CSL} can be written as $\eta_{CSL}=A_1[\cos(\omega t-\phi_1)+A_2/A_1\cos(\omega t-\phi_2)]$, where $A_1$and A_2 are the amplitudes for the waves traveling across the mouth of the GC and around the GC, respectively, ω is the angular frequency, t is the time, ϕ_1 is the phase lag for the wave traveling across the mouth and ϕ_2 is the phase lag for the wave traveling around the gulf. Representative values for ϕ_1 and ϕ_2 were taken from the coherence spectra between MZN-SFQ and the time that a 60 day period wave would take to travel from MZN to CSL (traveling into the GC) based on the phase speed calculated from correlation functions (see section 3.2). Phases are such that $\phi_1 < \phi_3 < \phi_2$.

The wave amplitudes A_1 and A_2 are, in general, different since both waves will be subject to different dissipation and/or scattering as they travel their different paths. Since the phase of the resulting wave at CSL depends on the ratio A_2/A_1, the lag of maximum correlation and the phase spectra will also depend on this ratio. Indeed, for certain combinations of amplitudes one can obtain a zero phase lag for the cross-correlation function and coherence function between the two signals described above. In testing this very simple model, some red noise was added to make things more realistic.

Acknowledgments

The authors wish to thank the crew of the B/O Francisco de Ulloa and R/V Point Sur. F. Miranda, A. Ledo, F. Plaza, C. Flores, C. Morales, M. Stone, R. Blanco, S. Larios, L. F. Navarro, and E. Gil provided help during fieldwork. This work was funded by CONACyT through grants G33464-T, 38797-T, C01-25343, ESE-203401, and through a scholarship to M. O. Gutiérrez. Comments by two anonymous reviewers improved earlier versions of this manuscript. English revisions by A. Spears are greatly appreciated.

References

Atlas, R., R. N. Hoffman, J. Ardizzone, S. M. Leidner, J. C. Jusem, D. K. Smith, and D. Gombos (2011), A cross-calibrated, multiplatform ocean surface wind velocity product for meteorological and oceanographic applications, *Bull. Am. Meteorol. Soc.*, *92*, 157–174, doi:10.1175/2010BAMS2946.1.

Baumgartner, T. R., and N. Christensen Jr. (1985), Coupling of the Gulf of California to large-scale interannual climatic variability, *J. Mar. Res.*, *43*(4), 825–848.

Bendat, J. S., and A. G. Piersol (1986), *Random Data: Analysis and Measurements Procedures*, Wiley Interscience, N. Y.

Bray, N. A. (1988), Thermohaline circulation in the Gulf of California, *J. Geophys. Res.*, *93*(C5), 4993–5020.

Castro, R., M. F. Lavín, and P. Ripa (1994), Seasonal heat balance in the Gulf of California, *J. Geophys. Res.*, *99*(C2), 3249–3261.

Christensen, N., Jr., R. de la Paz, and G. Gutierrez (1983), A study of sub-inertial waves off the west coast of Mexico, *Deep Sea Res., Part A*, *30*, 835–850.

Enfield, D. B. (1987), The intraseasonal oscillation in Eastern Pacific sea levels: How is it forced?, *J. Phys. Oceanogr.*, *17*, 1860–1876.

Enfield, D. B. and J. S. Allen (1983), The generation and propagation of sea level variability along the Pacific coast of Mexico, *J. Phys. Oceanogr.*, *13*, 1012–1033.

Gjevik, B., and M. A. Merrifield (1993), Shelf-sea response to tropical storms along the west coast of Mexico, *Cont. Shelf Res.*, *13*, 25–47.

Kundu, P. K. (1976), An analysis of inertial oscillations observed near Oregon coast, *J. Phys. Oceanogr.*, *6*, 879–893.

Large, W. G., and S. Pond (1981), Open ocean momentum flux measurements in moderate to strong winds, *J. Phys. Oceanogr.*, *11*, 324–336.

Lavín, M. F., and S. Organista (1988), Surface heat flux in the northern Gulf of California, *J. Geophys. Res.*, *93*(C11), 14,033–14,038.

Lavín, M. F., R. Castro, E. Beier, and V. M. Godínez (2013), Mesoscale eddies in the southern Gulf of California during summer: Characteristics and interaction with the wind stress, *J. Geophys. Res.*, *118*, 1367–1381, doi:10.1002/jgrc.20132.

Limeburner, R. (Ed.) (1985), CODE-2: Moored array and large-scale data report, Tech. Rep. 85-35, 234 pp., Woods Hole Oceanogr. Inst., Woods Hole, Mass.

López, M., and J. García (2003), Moored observations in the northern Gulf of California: A strong bottom current, *J. Geophys. Res.*, *108*(C2), 3048, doi:10.1029/2002JC001492.

López, M., J. Candela, and M. L. Argote (2006), Why does the Ballenas Channel have the coldest SST in the Gulf of California?, *Geophys. Res. Lett.*, *33*, L11603, doi:10.1029/2006GL025908.

López, M., J. Candela, and J. García (2008), Two overflows in the Northern Gulf of California, *J. Geophys. Res.*, *113*, C08023, doi:10.1029/2007JC004575.

Martínez, J. A., and J. S. Allen (2004a), A modeling study of coastal-trapped wave propagation in the Gulf of California. Part I: Response to remote forcing, *J. Phys. Oceanogr.*, *34*, 1313–1331.

Martínez, J. A., and J. S. Allen (2004b), A modeling study of coastal-trapped wave propagation in the Gulf of California. Part II: Response to idealized forcing, *J. Phys. Oceanogr.*, *34*, 1332–1349.

Merrifield, M. A. (1992), A comparison of long coastal-trapped wave theory with remote-storm generated wave events in the Gulf of California, *J. Phys. Oceanogr.*, *22*, 5–18.

Merrifield, M. A., and C. D. Winant (1989), Shelf circulation in the Gulf of California: A description of the variability, *J. Geophys. Res.*, *94*(C12), 18,133–18,160.

Pawlowicz, R., R. Beardsley, and S. Lentz (2002), Classical tidal harmonic analysis including error estimates in MATLAB using T_Tide, *Comput. Geosci.*, *28*, 929–937.

Ripa, P. (1997), Toward a physical explanation of the seasonal dynamics and thermodynamics of the Gulf of California, *J. Phys. Oceanogr.*, *27*, 597–614.

Romea, R. D., and J. S. Allen (1984), The effect of friction and topography on coastal internal Kelvin waves at low latitudes, *Tellus, Ser. A*, *36*(4), 384–400.

Spillane, M. C., D. B. Enfield, and J. S. Allen (1987), Intraseasonal oscillations in sea level along the west coast of the Americas, *J. Phys. Oceanogr.*, *17*, 313–325.

Zamudio, L., H. E. Hulburt, E. J. Metzger, and C. E. Tilburg (2007), Tropical wave-induced oceanic eddies at Cabo Corrientes and the María Islands, Mexico, *J. Geophys. Res.*, *112*, C05048, doi:10.1029/2006JC004018.

Zamudio, L., P. J. Hogan, and E. J. Metzger (2008), Summer generation of the Southern gulf of California Eddy train, *J. Geophys. Res.*, *113*, C06020, doi:10.1029/2007JC004467.

Zamudio, L., E. J. Metzger, and P. J. Hogan (2010), Gulf of California response to Hurricane Juliette, *Ocean Modell.*, *33*, 20–32, doi:10.1016/j.ocemod.2009.11.005.